university of groningen / faculty of mathematics and natural sciences

Advanced device structures for enhanced organic solar cell efficiencies

Master thesis

Laaya Shaabani

Supervisors:

Prof. Dr. Ir. P. W. M. Blom

Dr. Paul. de. Bruyn

Referent:

Dr. Remco Havenith

July 2012

Molecular Electronics, Physics of Organic Semiconductors

Zernike Institute for Advanced Materials

University of Groningen

Abstract

A Tandem or multi-junction solar cell, consisting of multiple layers in which two or more cells with different absorption spectra, i.e., different band gaps, are stacked, can overcome the limitations of a single-layer bulk heterojunction photovoltaic cell and can cover a larger part of the solar flux and allow utilizing the photon energy more efficiently. In this study, examples of organic tandem photovoltaic device architectures, geometries, and materials combinations that result in good performance are presented. The MoO_3/Ag/ MoO_3 intermediate layer, deposited between the active layers, proves to be a suitable transparent anode for fabricating organic tandem cells. We show that an increased Ag film thickness leads to a closed layer after the first cell deposition and the key advantage of our structure is that the processing steps do not affect the integrity of previously deposited layers.

Contents

GLOSSARY

HOMO	Highest occupied molecular orbital
LUMO	Lowest unoccupied molecular orbital
HTL	Hole transporting layer
ETL	Electron transporting layer
MPP	Maximum power point
V_{oc}	Open-circuit voltage
J_{sc}	Short-circuit current
FF	Fill factor
IPCE	Incident photon-to-current conversion efficiency
P3HT	Poly(3-hexylthiophene)
PCBM	[6,6]-phenyl-C_{61}-butyric acid methyl ester
PCPDTBT	poly[2,6-(4,4-bis-(2-ethylhexyl)-4*H*-cyclopenta[2,1-*b*;3,4-*b'*]dithiophene)-*alt*-4,7-(2,1,3-benzothiadiazole)]
ZnO	Zinc oxide
MoO_3	Molybdenum trioxide
ITO	Indium tin oxide
PEDOT:PSS	poly(3,4-ethylenedioxythiophene):poly(4-styrenesulfonate)
OLED	Organic light emitting diode
BHJ	Bulk heterojunction photovoltaic cell
EQE	External quantum efficiency

1 Introduction

The growing need for energy by the human society and depletion of conventional energy sources demands a renewable, safe, infinite, low-cost and omnipresent energy source. One of the most suitable ways to solve the foreseeable world's energy crisis is to use the power of the sun. Photovoltaic devices are especially of wide interest as they can convert solar energy to electricity. Most solar cells are based on polycrystalline silicon and have a relatively high cost price determined by the costs of the starting material and the expensive manufacturing process. In the last years, the development of solar cells based on organic molecules [1–3] and conjugated polymers [4–6] has progressed rapidly which are a good alternative for the silicon-based solar cells due to their potentially low manufacturing costs, light weight and ease of processing. One limiting parameter compared to more efficient, traditional silicon based devices is the low efficiency which limits the use of organic solar cells in industry. To make polymer based solar cells an economically interesting alternative, the efficiency of these devices must be increased. One possible way to improve the efficiency is by using a tandem configuration in which two or more cells with different absorption spectra, i.e., different band gaps, are stacked. This increases the absorption of solar light and allows utilizing the photon energy more efficiently [7].

The organic or polymer "tandem cell" architecture is a multilayer structure that is equivalent to two photovoltaic cells, in which a transparent intermediate layer is positioned between the two active layers. This transparent intermediate layer provides electrical contact between the two cells via efficient recombination of the holes and electrons created in the different sub-cells without voltage loss.

2 Theory

2.1 Conjugated polymers

Heeger, MacDiarmid and Shirakawa demonstrated in 1977 that chemical doping of conjugated polymers results in an increase of electronic conductivity by several orders of magnitude. This discovery was awarded with the Nobel Prize in chemistry in 2000 [8,9]. Most organic semiconductor materials are conjugated polymers which consist essentially of a linear framework of alternating single and double bonds between the carbon atoms along the polymer backbone. Conjugated polymers are nowadays used in various applications, like transistors, photodiodes, light emitting diodes, solar cells, etc. The origin of the conductivity and semi-conductivity behavior in conjugated polymers, e.g. polyacetylene, is because of having alternation of single and double bonds in their molecular structure which is a result of chemical bonding behavior of the carbon atoms (see Figure. 1.1).

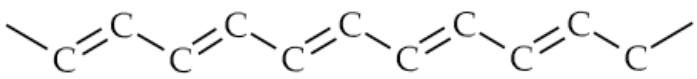

Figure 1.1. The chain of the carbon atoms with the alternating single and double bonds.

The carbon atom, in the ground state, has four valence electrons, 2 in 2*s* and 2 in 2*p* orbitals. In conjugated polymers carbon atoms are sp^2 hybridized. In the sp^2 hybridization the 2s orbital is hybridized with two 2p orbitals ($2p_x$, $2p_y$) giving rise to three sp^2 orbitals and one 2p orbital ($2p_z$) is left. Carbon can form two types of bonds: the σ-bond is formed by the overlap of the hybridized orbitals of the adjacent atoms which are oriented along the chain. So there are three coplanar sp^2 hybridized orbitals which are at an angle of 120° with each other. Therefore three σ bonds are formed, two with neighboring carbon atoms and one with a hydrogen atom. The remaining out of plane P_z orbitals, each occupied by one electron, overlap with neighboring P_z orbitals to form π bonds which are perpendicular to the chain shown. These electrons are delocalized along the entire

polymer backbone, which is the reason for the conducting properties of conjugated polymers.

The overlap of p_z orbitals forms two molecular orbitals, a bonding π-orbital which is the highest occupied molecular orbital (HOMO) and an antibonding π*- orbital which is the lowest unoccupied orbital (LUMO). The π-orbital and π*- orbital are equivalent to the valence band and conduction band of an inorganic semiconductor, respectively. The difference between the HOMO and LUMO is called the band gap of the organic material. The optical and electrical properties of an organic material are determined by the band gap. The gap is reduced when the polymer chain is longer. The chemical structure and schematic drawing of ethylene is illustrated in Figure 1.2, which is the simplest example of a conjugated molecule.

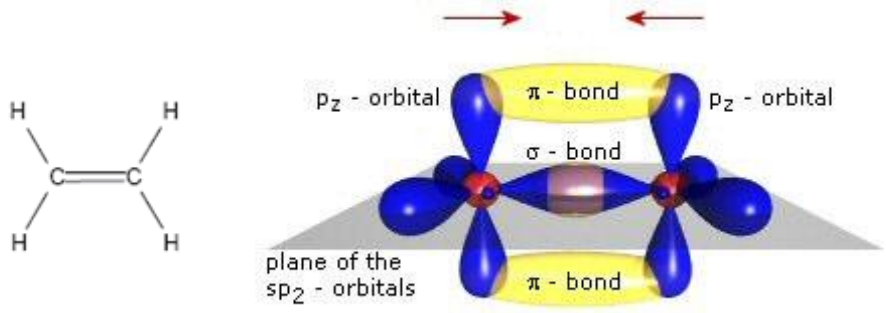

Figure 1.2. Chemical structure and schematic drawing of ethylene.

2.2 Organic solar cells

2.2.1 Working principles of organic solar cells

Organic solar cells are built from thin films of organic semiconductors. The most important difference between solar cells based on inorganic and organic semiconductors is that in inorganic solar cells, photons are directly converted into free charge carriers. Then the charge carriers can be collected by the corresponding electrodes. In organic photovoltaic devices, photoexcitation of a molecule leads to creation of excitons. The principle of an organic solar cell is depicted in Figure 1.3. Photons which are transmitted by a transparent electrode, are absorbed by the active material and excite the donor material, leading to the creation of excited electron–hole pairs (excitons). These electron-hole pairs are coulombically bound and can relax back to the ground state by multiple pathways. One of the pathways is the route in which charge carriers are created. The created excitons diffuse within the donor phase until they encounter the interface with the acceptor.

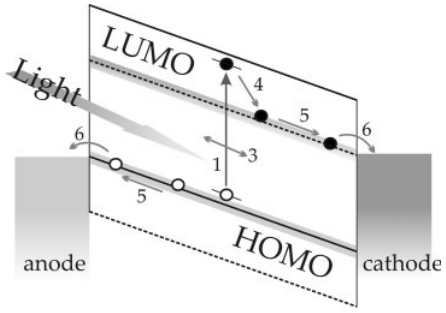

Figure 1.3. : Principle of a polymer based solar cell. The incoming (sun) light is transmitted by a transparent electrode. The organic layer between the transparent and the metal electrode consists of a donor and acceptor material. Absorbed photons create an exciton on the polymer chain that can result in the formation of charge carriers (electron and hole). The charge carriers drift to the corresponding electrode creating a current. The dashed line represents the energy levels of the acceptor, while the full lines indicate the energy level of the donor in the PV cell. HOMO: highest occupied molecular orbital; LUMO: lowest unoccupied molecular orbital[10].

Dissociation then takes place via an ultrafast charge transfer (45 fs) from the excited donor to the acceptor, leading to charge separation. Subsequently, photo-generated holes and electrons are transported through the donor and acceptor phases towards the electrodes (anode and cathode) with the aid of the internal electric field, caused by the use of electrodes with different work functions. Finally they are collected by the electrodes, creating a current in the photovoltaic device.

A typical bulk heterojunction photovoltaic cell has a geometry as depicted in Figure 1.4. The photoactive material is sandwiched between a high and low work function electrode, one transparent and one reflecting. The glass substrate coated by indium-tin-oxide (ITO), which has a high work function and is a transparent conductive electrode, used as an anode and makes an ohmic contact with the highest occupied molecular orbital (HOMO) of the donor material. The cathode material on top which is a low work function metal with or without lithium fluoride makes an ohmic contact with the lowest unoccupied molecular orbital (LUMO) of the acceptor material. A layer of PEDOT:PSS is spin casted to reduce the roughness of the ITO and increase the work function.

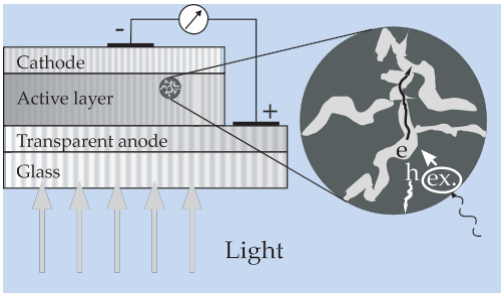

Figure 1.4. A typical BHJ solar cell geometry. The enlarged part of active material shows the processes of light absorption and charge transport.

2.2.2 Characteristics of organic solar cells

In order to determine the ability of a photovoltaic device to convert incident photon energy into electrical energy, current- voltage characteristics are measured, both in dark and under illumination.

A typical current-voltage characteristic of a solar cell is displayed in Figure 1.5. In dark conditions, solar cells ideally operate as a diode. Under illumination the device generates current. Short circuit current density (J_{sc}) is the current density under illumination at zero potential difference between anode and cathode. Under short-circuit conditions, the Fermi-Level of the two electrodes align. J_{sc} is found at the intersection of the curve and the vertical axis. Open-circuit voltage (V_{oc}) is the maximum voltage that can be generated by the device. At this voltage current density under illumination is zero and is found where the curve intersects the horizontal axis.

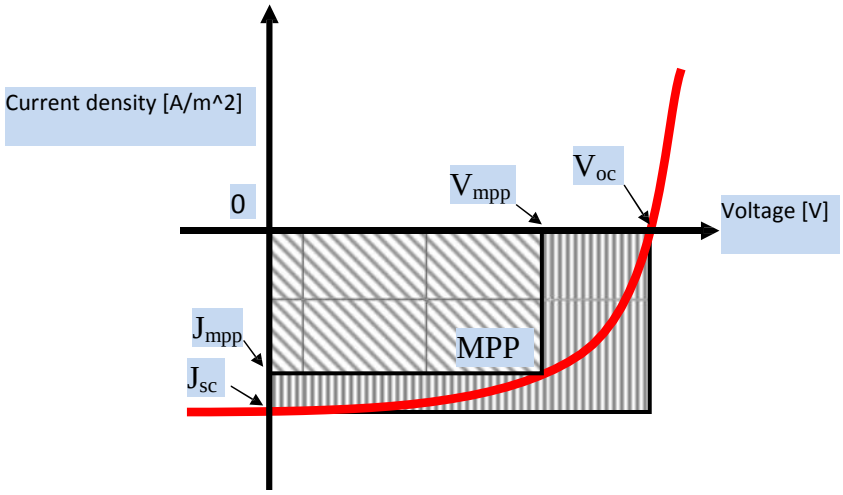

Figure 1.5. A typical J-V characteristic of a solar cell with indication of the short-circuit current density (J_{sc}), the open-circuit voltage (V_{oc}), and the maximum power point (*MPP*) with the corresponding current density (J_{mpp}) and voltage (V_{mpp}).

The maximum power point (MPP) is defined as the point where the product of current density and voltage is maximized. The J-V curve gives us the Fill factor (FF) which is defined as the ratio between P_{MPP} and the theoretically maximum power of the device (P_{max}):

$$FF = \frac{V_{max} \times J_{max}}{V_{oc} \times J_{sc}}$$

where V_{max} and J_{max} are the voltage and current density in the MPP respectively.
The power conversion efficiency for a solar cell is defined as follows:

$$\eta = \frac{P_{out}}{P_{in}} = \frac{FF \times V_{oc} \times J_{sc}}{P_{in}}$$

where P_{in} is the power density of the incident light and P_{out} is the electric power generated by the cell at the maximum power point. The incident light power density is usually standardized to the AM 1.5G spectrum.

2.3 Tandem solar cells

2.3.1 Limitation of solar cells efficiency

Solar cell efficiency is limited by two main reasons: losses by thermalisation and non-absorption of low-energy-photons (Transmission loss). In the case of thermalisation loss, photons with energies larger than band gap of the semiconductor will lose their excess energy via thermal equilibration. For transmission losses, the energy barrier between HOMO and LUMO is too high for photon absorption and photons with energies smaller than the band gap cannot be absorbed. Figure 1.6 illustrates this statement. Multiple junction (tandem) solar cells are used to improve the efficiency of organic photovoltaic devices. In this way, single heterojunction cells are stacked on top of each other to form a multilayer structure. One material should then collect the higher energetic photons and the other, with a lower band gap than the first one, should absorb photons with lower energy. The combination of a wide and small band gap polymer for a tandem solar cell improves use of photon energy and enables wider coverage of the solar spectrum.

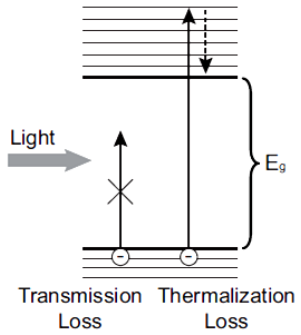

Figure 1.6. Transmission loss and thermalization loss.

2.3.2 The structure of an organic tandem solar cell

The device structure of an organic tandem solar cell is depicted in Figure 1.7. There are two methods to stack sub-cells: parallel or serial connections. The most common multi-junction solar cell employs a two-terminal series configuration by stacking two active layers. The requirement for this configuration is just having thin, non-absorbing metallic or semiconducting layers to separate the different cells and act as recombination layer. For parallel connections, it is required to have intermediate electrodes which ensure efficient charge collection for each cell. In order to minimize photon losses and maximize charge carrier collection, these electrodes have to be transparent and highly conducting. An obvious material for such an electrode would be indium tin oxide (ITO). However, ITO is usually deposited via reactive sputtering which might severely damage the conjugated polymer. Therefore, such parallel connections are not easily achievable in the case of organic semiconductor solar cells[11].

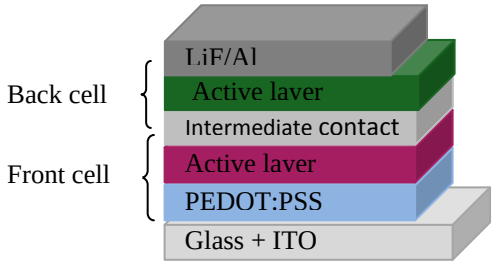

Figure 1.7. Device structure of an organic tandem solar cell.

In the case of a series-connection, the intermediate layer acts as a recombination site, allowing holes from the HOMO of the back cell to recombine with electrons from the LUMO of the front cell. When the sub-cells are connected in series, the same current has to flow through the entire device (current matching). This current is limited by the lower current of the two sub-cells, which for organic semiconductors in most cases is the top cell. This means that the overall generated power is limited by the lowest generated power in the configuration. If one of the sub-cells generates much more current than the

other, excess charges will be pile up at the intermediate layer and cannot contribute to the photocurrent. These charges generate an electric field and thus compensate for the built-in potential across the sub cell[12]. This compensation leads to a reduced fillfactor in the tandem cell[13,14].

To avoid such situations, optimization of the respective cell thickness has to be performed which is a challenge[11]. With two sub-cells stacked in series, the voltage of a tandem cell is determined by the addition of the voltages of the sub-cells. In the case of a parallel connection, the short circuit current of the cells are summed up and the V_{oc} is driven by the smallest cell voltage.

3 Experimental

3.1 Materials

3.1.1 Glass and ITO

All the devices considered in this study were fabricated glass coated with Indium Tin Oxide (ITO, or tin-doped indium oxide). Glass can be used as a substrate for making samples because of its flatness, rigidity and its transparency in the spectral range of interest, i.e. visible and near-infrared. Indium tin oxide is a solid solution of indium(III) oxide (In_2O_3) and tin(IV) oxide (SnO_2), typically 90% In_2O_3, 10% SnO_2 by weight. Since ITO has high electrical conductivity and high optical transparency, it is one of the most widely used transparent conducting oxides. Furthermore, it has a high work function of ~4.8 eV, which makes it very suitable as a hole-extracting electrode[15]. Since ITO has high atmospheric stability and insolubility, it can be used in wet processing conditions during cleaning and spin coating.

3.1.2 Poly(3-hexylthiophene)

Poly(3-hexylthiophene) (P3HT) is the most studied polymer for organic photovoltaic applications. It has been widely researched and used as donor in organic solar cells. It has a high hole mobility of about $1.3*10^{-8}$ cm^2/Vs. It is a high band gap polymer (1.9 eV), its HOMO lies at -4.8 eV, the LUMO at -2.9 eV. The chemical structure of this polymer is shown in Figure 1.8.

3.1.3 PCPDTBT

Poly[2,6-(4,4-bis-(2-ethylhexyl)-4H-cyclopenta[2,1-b;3,4-b']dithiophene)-alt-4,7-(2,1,3-benzothiadiazole)] (PCPDTBT) is a narrow band-gap material which has an optical band-gap of approximately 1.7 eV. It has energy levels of -5.3 eV and -3.6 eV for the HOMO

and LUMO respectively. The molecular structure of this polymer is depicted in Figure 1.8.

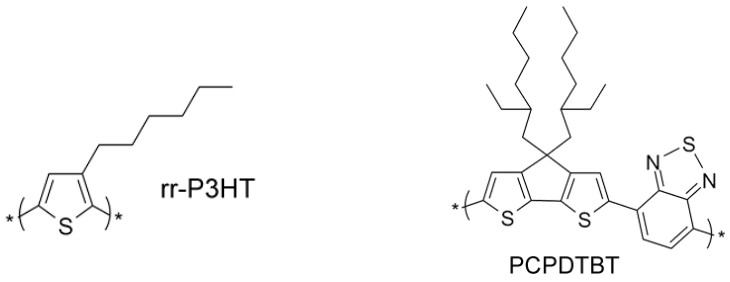

Figure 1.8. The chemical structure of organic donor materials used in this study. Depicted are the monomer units of the polymers P3HT and PCPDTBT.

3.1.4 [6,6]-phenyl-C61-butyric acid methyl ester

[6,6]-phenyl-C61-butyric acid methyl ester (PCBM) is a derivative of the Buckminsterfullerene (C60) molecule and is generally used as electron acceptor molecule. The chemical structure of this molecule is shown in Figure 1.10. This molecule has a high electron affinity, relatively good conductivity and large band gap of ~2.3 eV. PCBM is significantly highly soluble in chlorobenzene, toluene, chloroform and similar organic solvents which make it suitable to solution-based processing methods such as spin coating. It has energy levels of -6.1 eV for the HOMO and -3.8 eV for the LUMO.

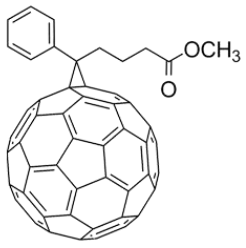

Figure 1.10. The chemical structure of PCBM.

3.1.5 Aluminium and lithium fluoride

Aluminium is used as the low work function cathode in this study. Since its work function (4.3 eV) is deeper in energy than the LUMOs of all the materials mentioned above, it is a suitable electron extracting material. Tang et al. reported that adding a thin (~1nm) layer of LiF in between the active layer and the aluminium electrode improves device performance[16,17]. Adding this interstitial layer increases device lifetime and prevents the formation of trap states due to oxidation of the Al interface.

3.1.6 PEDOT:PSS

PEDOT:PSS, poly(3,4-ethylenedioxythiophene) doped with poly(styrenesulfonate), is a stable, water soluble conjugated polymer which is used as a hole transporting layer. A layer of PEDOT:PSS (work function ~5.2 eV) is spin cast to reduce the roughness of the ITO and improve the work function of the ITO-layer. Furthermore, it can be used to match the highest occupied molecular orbital (HOMO) of the donor. The PEDOT:PSS also improves the wetting for the processing of the active layer of the solar cell. The chemical structures of PEDOT and PSS are depicted in Figure 1.11.

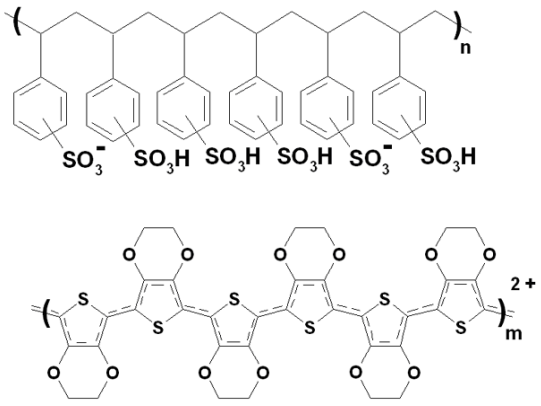

Figure 1.11. The chemical structure of PEDOT and PSS

3.1.7 Chloroform

Chloroform is an organic compound with formula $CHCl_3$ which is a colorless solvent and has a high vapor pressure among organic solvents and high solubility for a wide range of organic materials, including PCBM, P3HT, PCPDTBT. It is relatively unreactive and conveniently volatile and because of its low boiling point (61.2^{o} C) and volatility, it dries quickly and makes processing time short. Therefore, it can be used for solution based methods such as spin coating.

3.1.8 Zinc oxide

Zinc oxide (ZnO) as a low work function material (~4.2 eV) can be used as a cathode. This semiconductor has several favorable properties, including good transparency, high electron mobility and wide bandgap. Those properties are used in emerging applications for transparent electrodes in inverted solar cell structures[18-20] and organic tandem solar cell devices[7].

3.1.9 Molybdenum trioxide

Molybdenum trioxide (MoO_3) as a high work function material (~6.7 eV) can be used in photovoltaic devices as the transparent anode. A layer of molybdenum trioxide serves as a hole transport and charge collecting layer. It can effectively substitute PEDOT:PSS as the buffer layer in the polymer PV cells.

3.2 Device fabrication

3.2.1 Substrate preparation

The substrate consists of a piece of glass of dimensions 3×3 cm coated with ITO. Each sample was first scrubbed manually with a warm (~50^{o}C) solution of soap and de-ionized water, followed by ultrasonic treatment in acetone and 2-isopropanol to remove any organic materials. Afterwards they were dried in an oven at 140^{o} C for 10 min in ambient conditions, followed by UV-ozone treatment for 20 min. During the cleaning procedure, the substrate was constantly kept in a class 1,000 air flow (ISO 7).

3.2.2 Solution preparation

In order to prepare the solutions, P3HT:PCBM (1:0.8 by weight, 15 mg/mL of polymer) was dissolved in chloroform and PCPDTBT:PCBM (1:4 by weight, 3.5 mg/mL of polymer) was dissolved in a chloroform solution and left to stir overnight. For preparing zinc oxide layers, 20 mg/mL of $Zn(acac)_2$ hydrate (obtained from Sigma–Aldrich) was dissolved in absolute ethanol under ambient conditions. This is followed by prolonged stirring using magnetic stir-bars on a magnetic plate for several hours at 50^{o} C and subsequently filtering with a 0.2 μm pore size PTFE filter. Polymer solutions were filtered with a 0.45 μm pore size PTFE filter to extract any aggregates or impurities from the solution.

3.2.3 Spin coating of the active layer

Spin coating is a commonly used processing method for deposition of the active layer of the solar cell which is used to produce uniform thin films on substrates. The thickness and quality of the active layer are determined by the type of solvent, solution concentration, spin duration and acceleration speed. Spin casting of the P3HT:PCBM and PCPDTBT:PCBM blends was done in a nitrogen atmosphere in a glovebox, constantly filtering out oxygen and water to strictly maintain levels of <0.1 ppm O_2 and H_2O. In order to enhance the efficiency of photovoltaic devices, spin coating of the P3HT:PCBM layers was followed by an annealing step at 140^{o} C for 15 minute.

3.2.4 Tandem cell processing

In order to make an organic tandem solar cell containing two sub-cells in a parallel configuration two sub-cells are stacked on top of each other. This configuration does not have the problem of optimization of the layer thickness of the sub-cells in a serial configuration. Therefore a parallel tandem solar cell can potentially lead to a higher performance compared to the tandem solar cell connected in series. The proposed geometry for this tandem cell is an inverted structure with P3HT:[60]PCBM as wide band gap front cell and a conventional structure with PCPDTBT:[60]PCBM as small band gap back cell. An intermediate layer is considered between these two sub-cells. The requirement for this purpose is that the intermediate layer be thick enough to prevent impairment of the first active layer during processing of the second active layer. Another requirement is that this separating layer has to be as transparent as possible to transmit light efficiently to the second cell.

3.2.5 Usage of ZnO/Ag/ZnO as cathode

The first tandem system of interest is a device consisting of a ZnO/Ag/ZnO middle contact to separate and connect the two sub-cells. This layer serves as an electron transport (cathode) and charge collecting layer for the first cell and at the same time as the cathode of the second cell. For making these kind of devices, a glass substrate patterned with a sputtered ITO layer of approximately 140 nm was spin cast on by a layer of PEDOT:PSS (typically Clevios P VP AI 4083) in air to yield a 50 nm layer on the substrate. After spin coating of the active material of the front cell, to make a layer of ZnO, a simple, low temperature solution process was used[21]. $Zn(acac)_2$ was spin cast in air at 1000 rpm, while both solution and substrates were held at 50^{o} C. This was followed by pyrolysis of the precursor material zinc acetylacetonate ($Zn\ (acac)_2$) hydrate in air during 30 s on a hotplate at 120^{o} C. After thermal evaporation of Ag (~6nm) at a pressure of 10^{-6} mbar, a layer of ZnO was considered on top. The next step of the procedure of building up the tandem cell structure is spin coating of the second active layer. Finally, the process can be finished by thermal evaporation of the anode, consisting of a 10 nm layer of MoO_3 followed by 100 nm of aluminium at high vacuum (approximately 10^{-4} Pa). MoO_3 powder was obtained from Sigma–Aldrich. The evaporation

rate was held constant at 0.05 nm/s and 0.01 nm/s to produce a smooth film of 10 nm and 1 nm for MoO_3 and LiF, respectively.

3.2.6 Usage of MoO_3/Ag/MoO_3 as anode

In this step the focus is on using MoO_3/Ag/MoO_3 as the intermediate layer. These devices are made using the same procedure as described before, so the devices have the same structure and differ only in the structure of the intermediate layer. Here, the MoO_3/Ag/MoO_3 middle layer serves as a hole transport (anode) and charge collecting layer for the first cell and at the same time as anode of the second cell. It serves as a stable foundation that enables the fabrication of the second cell to complete the tandem cell architecture. In this structure Zinc oxide (ZnO) as a low work function material was used as a transparent cathode on ITO coated glass. For making the MoO_3/Ag/MoO3 intermediate layer, a layer of MoO_3 (~10nm) was thermally evaporated on top of the active layer comprised of P3HT:PCBM, followed by thermal evaporation of Ag (~6nm). Then, a layer of MoO_3 (~20nm) was evaporated on top. Finally after spin coating of PCPDTBT:PCBM, 1 nm of lithium fluoride (LiF) and 100 nm aluminum (Al) were evaporated as a cathode.

3.3 Device characterization

3.3.1 J-V characteristics

The overall efficiency of a photovoltaic device is determined by measuring its current – voltage characteristic. Electrical characterization was performed using a computer-controlled Keithley 2400 SourceMeter in the dark and under illumination. The current standard for characterisation is simulation of the AM1.5G solar spectrum. The photovoltaic devices were illuminated using a Steuernagel SolarConstant 1200 metal-halide lamp calibrated to an intensity of 1 kW/m^2 (in accordance with standard testing conditions) by using a silicon reference photodiode. All measurements were performed at a temperature of 295 K (room temperature) and the temperature of the device was kept constant. ITO and Aluminum were connected to the positive and negative terminal, respectively. The current response was measured by continuously sweeping from -2 Volts to +2 Volts.

3.3.2 IPCE measurements

External quantum efficiency (EQE), is calculated from the spectral responsivity SR(λ) of the device over a range of wavelengths by

$$IPCE = \frac{hc}{q\lambda} SR(\lambda)$$

SR(λ), the spectral responsivity, is the ratio of the extracted current density to the incident power density at wavelength λ.

EQE is the ratio of the number of incident photons to the number of charge carriers extracted, and is also known as the Incident-photon to electron conversion efficiency or (IPCE). IPCE spectra were measured from 400 to 1100 nm using a custom-built setup consisting of a 50 W quartz tungsten halogen lamp (Newport Research Series), 33 narrow band-pass interference filters (CVI Laser) a transimpedance amplifier and a Stanford research Systems SR830 lock-in amplifier. The setup was calibrated using a Silicon (Newport 818-SL) and a Germanium (Oriel 71653) photodiode[22].

4 Results and Discussion

4.1 Optical properties of ZnO/Ag/ZnO

As a first step to start building an organic tandem cell, a ZnO/Ag/ZnO intermediate layer was developed. To obtain a better understanding of the working mechanisms of these devices, it is interesting to investigate their optical properties. Optical transmittance was measured in the range of 300-1500 nm with a Perkin-Elmer Lambda 900 spectrophotometer. Sheet resistance was measured using the four-point probe method.

.

4.1.1 Ag thickness

The relationship between the transmittance of a ZnO/Ag/ZnO multilayer film and wavelength for different thicknesses of the Ag layer is shown in Figure 4.1. Excellent optical transparency in the visible range of wavelengths was observed.

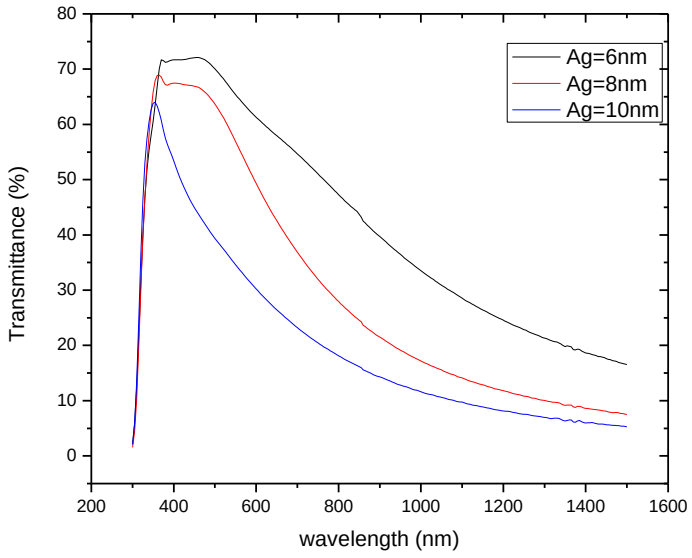

Fig. 4.1. Dependence of transmittance of ZnO/Ag/ZnO multilayer film on the Ag layer thickness.

The thickness of the Ag layer was varied from 6 to 10 nm. It is apparent in Figure 4.1. that at about 6 nm thick Ag layer, high transmittance values were obtained.

The transmittance of ZnO/Ag/ZnO film has a peak at 450-500 nm and the transmittance is greater than 60% over the entire visible light wavelength range. With increasing thickness of the Ag layer, the transmittance decreases and the reflection increases as the film becomes a mirror.

At about 6 nm thick Ag layer, the sheet resistance has reached value of 6 Ω/sq and does not change any more as the silver layer thickness is increased. For very thin Ag layers, the sheet resistance increases and transmittance decreases. This is due to the absorption in the aggregated Ag film. A continuous layer of Ag has low absorption and good electrical conductivity. From this result it is clear that 6 nm is the critical point and with a further decrease in the layer thickness beyond this point absorption of light and electrical resistivity rapidly increase. This behavior is attributed to a transition from a continuous film to the aggregated state (distinct islands of silver atoms). So, the optimum thickness of the silver layer for high optical transmittance and good electrical conductivity was determined to be 6 nm.

4.1.2 Ag evaporation rate

Figure 4.2 shows the dependence of transmittance of the ZnO/Ag/ZnO multilayer film on the Ag layer evaporation rate. The deposition rate was varied from 0.01 Å/s to 6 Å/s.

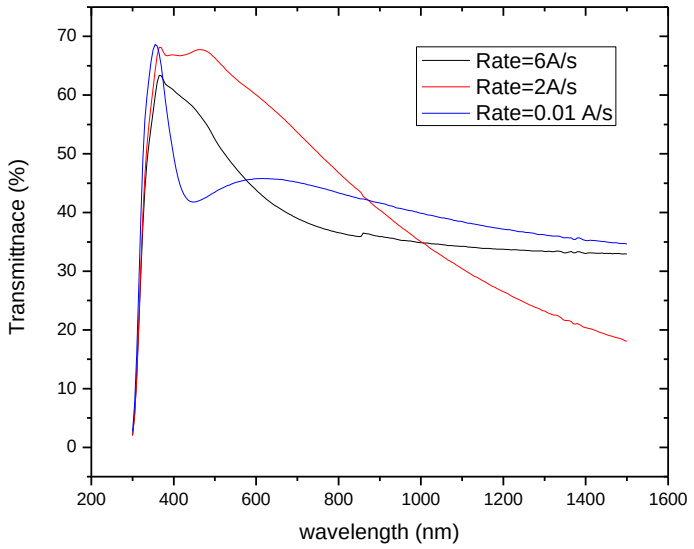

Fig. 4.2. Dependence of transmittance of ZnO/Ag/ZnO multilayer film on the Ag layer deposition rate.

It is seen from Figure 4.2 that at about 2 Å/s silver layer evaporation rate, high transmittance values were obtained.

In order to have high optical transmittance of the ZnO/Ag/ZnO multilayer at room temperature, the deposition rate of the Ag layer should be optimized.

4.1.3 Deposition angle

To investigate the effects of deposition angle, the substrates were placed in different positions of the deposition system. The results for transparency of the ZnO/Ag/ZnO multilayer film for different deposition angles for silver layer are shown in Figure 4.3. It is seen that for different positions of substrates in the deposition system, when the target-substrate distance is different and thus the deposition angle, also the transparency is different.

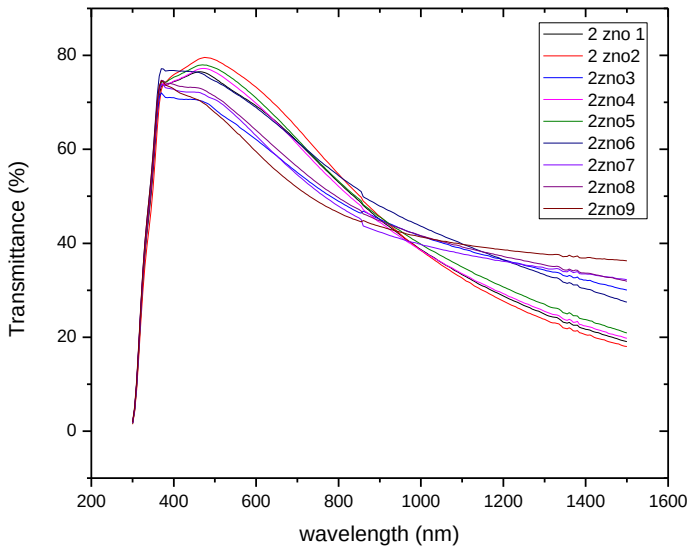

Fig. 4.3. Dependence of transmittance of ZnO/Ag/ZnO multilayer film on the deposition angle.

4.1.4 ZnO thickness

The transmittance of the ZnO/Ag/ZnO film for different thicknesses of the ZnO layer and for a constant silver layer thickness of 6 nm and constant deposition rate of 2 Å/s is presented in Figure 4.4. Each curve of this graph represents multilayers with different

thickness of the ZnO layer. The thickness of the ZnO layers was varied from 30 to 100. The ZnO layer thickness was measured with the Veeco Dektak 6M Profilometer. It is apparent in Figure 4.4. that when the thickness of ZnO layer is 70 nm, high transmittance values are obtained and the transmittance is greater than 70% over the entire visible light wavelength range.

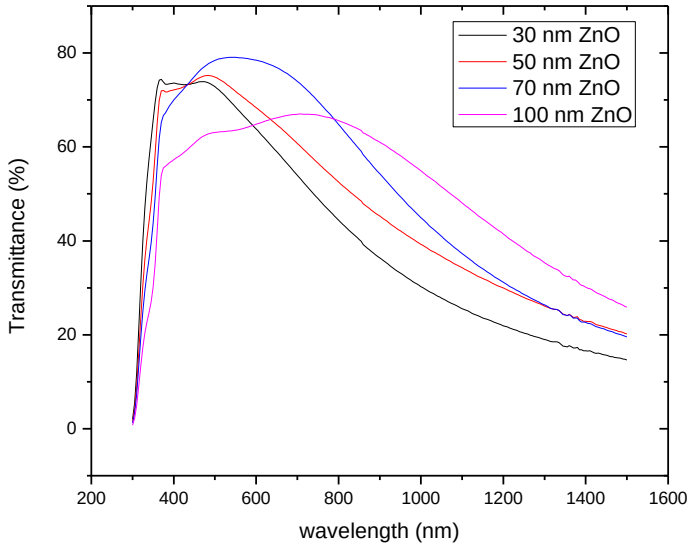

Figure 4.4. Dependence of transmittance of ZnO/Ag/ZnO multilayer film on the ZnO layer thickness.

We can therefore conclude that in order to have superior electrical and optical properties of the ZnO/Ag/ZnO multilayer at room temperature, optimization of the thicknesses of both the ZnO and the Ag layer and optimization of deposition rate and angle are necessary.

4.2 Organic tandem solar cells with ZnO/Ag/ZnO as intermediate layer

The most obvious way to start with organic tandem solar cells is to take the well known bulk heterojunction structure, make an intermediate layer, and spin-cast a second bulk heterojunction cell on this layer. As a first step, a double junction solar cell incorporating ZnO/Ag/ZnO as the intermediate layer was investigated. We used well-established material combinations for the active layers, employing blends of poly(3-hexylthiophene) (P3HT) or poly[2,6-(4,4-bis-(2-ethylhexyl)-4H-cyclopenta[2,1-b;3,4-b']dithiophene)-alt-

4,7(2,1,3- benzothiadiazole)], also known as PCPDTBT as electron donors mixed with a soluble fullerene derivative [6,6]-phenyl-C61-butyric acid methyl ester ([60]PCBM or PCBM in short) as electron acceptor dissolved in chloroform. The intended layout for this structure is shown in Figure 4.5.

Processing of the second active layer from a chloroform solution has been observed to induce a dissolution of the first layer. So the integrity of previously deposited layers was affected and cracks appeared in the whole layer stack as shown in Figure 4.6. This indicates that the solvent of the second active layer diffuses into the silver layer and destroys it. Thus, the silver layer is not continuous and subsequently there is no current. It appears clearly that the deposition of a second cell requires that the first one is protected towards dissolution.

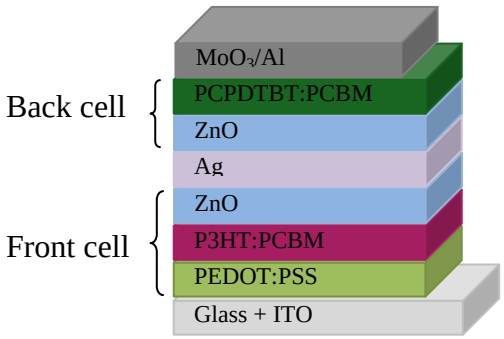

Figure 4.5. Device layout for a solution processed organic tandem solar cell.

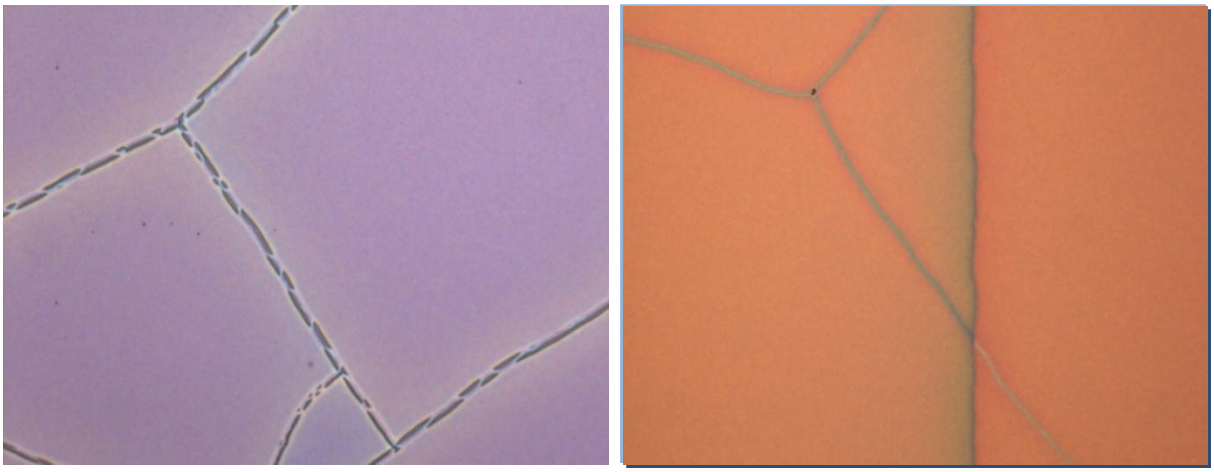

Figure 4.6. Optical microscope pictures of appeared cracks on substrate after second active layer spin-casting.

4.3 Single devices with ZnO

In order to improve the understanding of the working of the tandem cell, a single configuration solar cell was fabricated. ITO - coated glass with a PEDOT:PSS layer on top was used as substrate and P3HT:PCBM was spin coated from a chloroform solution. After spin coating of the ZnO layer, a Ag layer with a thickness of 6 nm was deposited on top. Finally contact pads of 100 nm Ag are evaporated onto the device, resulting in a device structure of ITO/PEDOT:PSS/P3HT:PCBM/ZnO/Ag The structure of the device is shown in Figure 4.7.

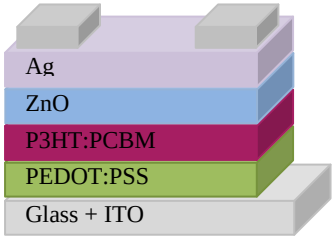

Figure 4.7. Device structure of studied single solar cells.

The results for comparison of current density to voltage (*J*–*V*) characteristics measurements are shown in Figure 4.8. It is clear from this figure that the resulting curve obtained from a 6 nm Ag layer is s-shaped around V_{oc}. This might be due to the fact that contact between Ag and ZnO is not ohmic. In the next step, the thickness of Ag was increased up to 100 nm. Several experiments showed that in contrast to 6 nm of silver, the structure with 100 nm silver performs significantly better and the efficiency is reasonable. We can conclude that single solar cells with thin Ag cathodes on ZnO show a contact problem compared to thick Ag cathodes and the problem is not to be found in series resistance, since the sheet resistance is very low.

To verify which metal would be the optimum in this structure, two different metals, namely silver and aluminum with different thicknesses of 6 and 100 nm, were used and results were compared. Since the Fermi levels of ZnO and Al align much better than Ag and ZnO, aluminum was selected for this structure to be compared with silver.

The results presented in Figure 4.9 reflect that thick metal films make good cathodes and in the case of 100 nm metal deposition, aluminum turned out to give slightly better results.

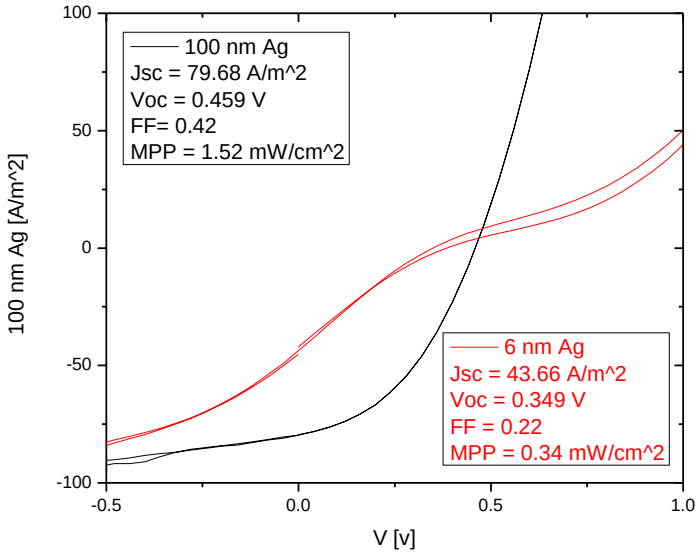

Figure 4.8. Comparison of Current density – voltage characteristics of single cells of P3HT:PCBM with 6 nm and 100 nm thickness of Ag layer.

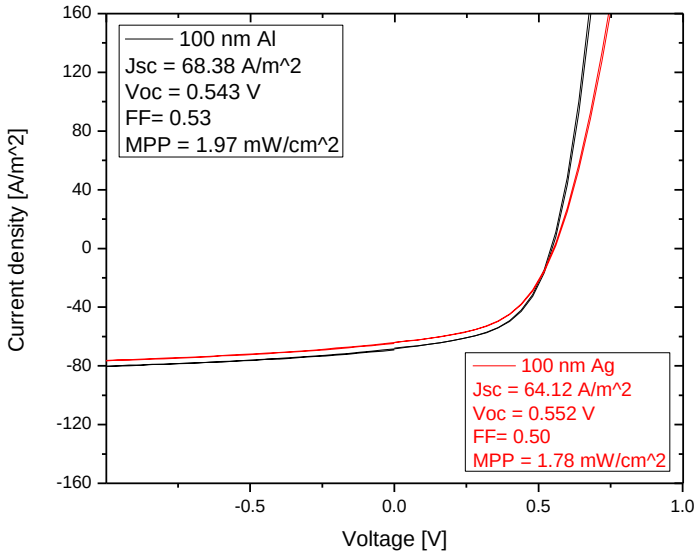

Figure 4.9. Comparison of Current density – voltage characteristics of single cells with 100nm layer thickness of Al and Ag.

Figure 4.10 shows that the thin Al film does provide ohmic contact, but has a large series resistance, evidenced by ohmic behavior throughout the characteristic. The sheet resistance of aluminum was measured and compare to silver. The sheet resistance for Al is 60 Ω/□ compared to 6 Ω/□ for Ag. Therefore, for the 6 nm Al layer, because of the high resistivity, the conductivity of Al is not good enough and the fill factor is quite low.

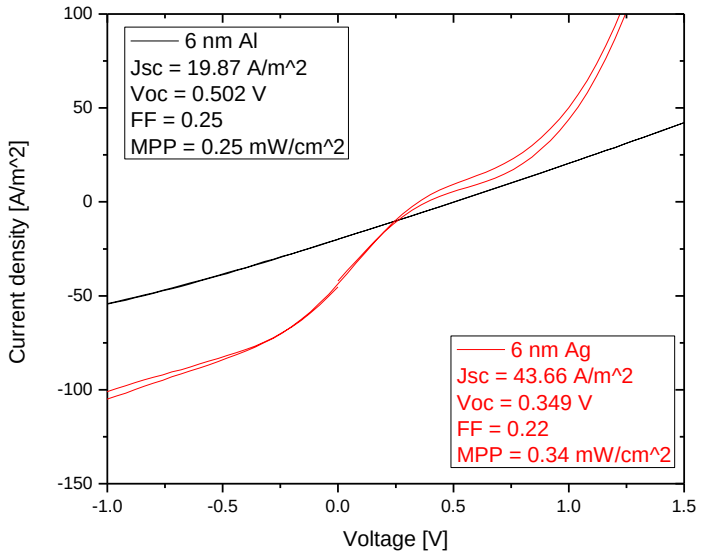

Figure 4.10. Comparison of Current density – voltage characteristics of single cells with 6 nm layer thickness of Al and Ag.

To determine the influence of the aluminum thickness on device performance, different devices with different thicknesses of aluminum were prepared, using the same fabrication procedure as described in section 3.2. Therefore, the devices differ only in the aluminum layer thickness. Table 4.1 shows the performance of several such devices. In Figure 4.11, the current density versus voltage curves are plotted for the different thicknesses of Al, ranging from 6 nm to 20 nm. These results show that a larger Al thickness decreases the series resistance and the percolation threshold for conduction seems to be 6-7 nm.

For the device with 10 nm aluminum thickness, a higher fill factor of 49% was observed, which is the highest fill factor recorded between these devices. Therefore, the optimum thickness of the aluminum layer for high performance was determined to be 10 nm.

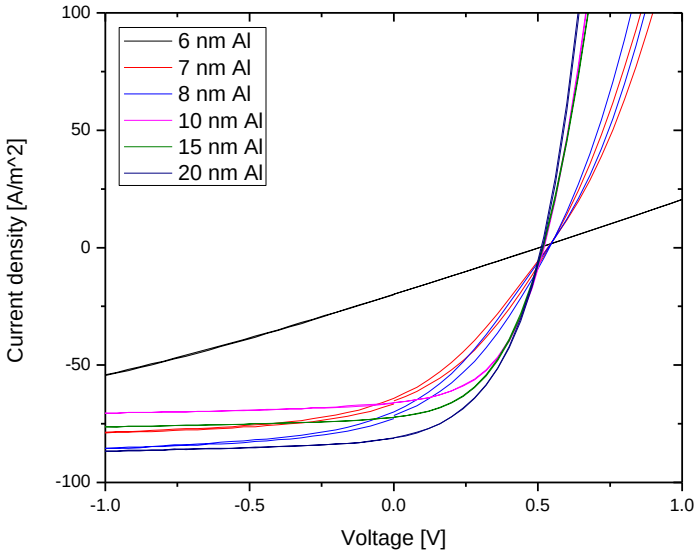

Figure 4.11. Comparison of Current density – voltage characteristics of single cells with 6, 7, 8, 10, 15 and 20 nm layer thickness of Al.

Thickness [nm]	Voc [V]	Jsc [A/m^2]	FF [%]	MPP [mW/cm^2]
6	0.502	19.87	25	0.25
7	0.534	64.17	32	1.10
8	0.536	69.95	32	1.21
10	0.519	66.01	49	1.68
15	0.515	72.28	47	1.73
20	0.511	81.00	45	1.87

Table 4.1: Device characteristics for various thickness of Al.

In order to investigate the transmittance of the ZnO/Al/ZnO layer, different devices with different rate of deposition for the aluminum layer were fabricated. Figure 4.12 shows the dependence of transmittance of the ZnO/Al/ZnO multilayer film on the Al layer evaporation rate. The deposition rate was varied from 0.2 Å/s to 2 Å/s. It is apparent in Figure 4.12 that at about 0.2 Å/s evaporation rate high transmittance values were obtained.

In the next step, to investigate the effects of deposition angle, substrates were placed in different positions of the deposition system. The results for the transparency of the ZnO/Al/ZnO multilayer film for different deposition angles for the aluminum layer are shown in Figure 4.13. The Al deposition rate shows the opposite of Ag, slower rates give better transmittance.

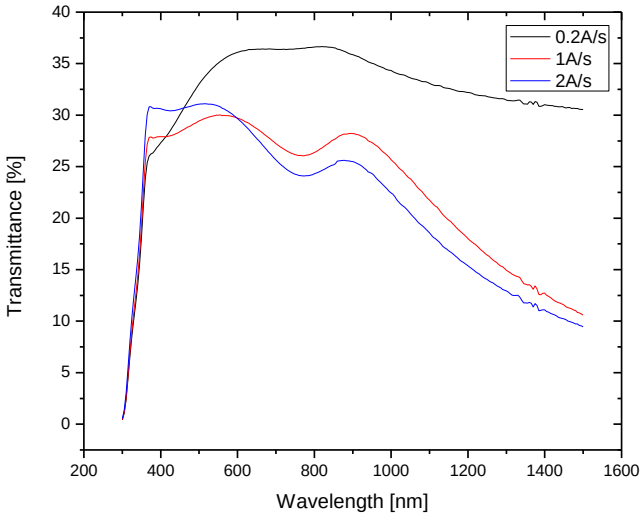

Fig. 4.12. Dependence of transmittance of ZnO/Al/ZnO multilayer film on the Al layer deposition rate.

To verify which metal would have the optimum transmittance in the ZnO/metal/ZnO structure as the intermediate layer, the two different metals, silver and aluminum were compared. The result of this comparison is shown in Figure 4.14. Comparing the different curves it is obvious that ZnO/Al/ZnO has a lower transmittance. Since the conductivity for this multilayer is also lower, as mentioned before, it was deemed an unsuitable combination for tandem solar cells.

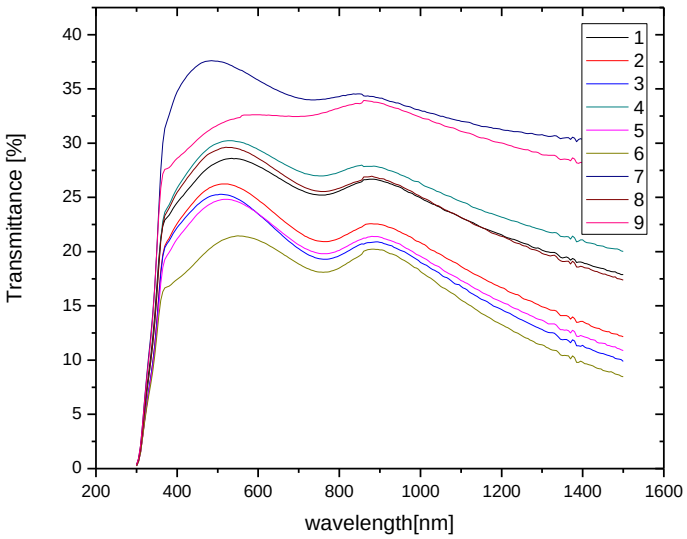

Fig. 4.13. Dependence of transmittance of ZnO/Al/ZnO multilayer film on the deposition angle.

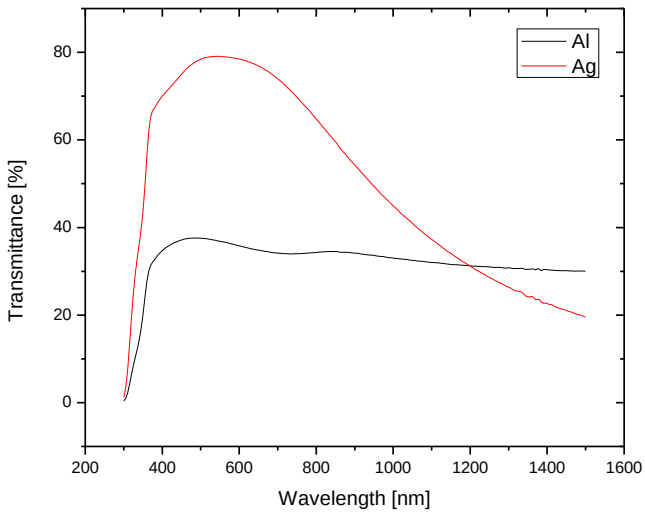

Figure 4.14. Comparison of the Transmittance of ZnO/metal/ZnO layer with two different metals, Silver and Aluminum.

4.4 Single devices with MoO_3

In the next step, single devices with MoO_3 were fabricated and the results were compared to single devices introduced in section 4.3. The proposed geometry for these devices is an inverted structure. ITO coated glass with a ZnO layer on top was used as substrate and P3HT:PCBM was spin cast from a chloroform solution. Next, a layer of MoO_3 of roughly 10 nm was deposited. This was followed by the deposition of a 6 nm Ag layer on top. Finally contact pads of 100 nm Ag are evaporated onto the device, resulting in a device structure of ITO/ZnO/P3HT:PCBM/ MoO_3/Ag.

Measuring the current density to voltage (*J–V*) characteristics of the sub-cells can result in a better understanding of the interplay between the two sub-cells. The result for the current density to voltage (*J–V*) characteristics measurement is shown in Figure 4.15. Introducing a MoO_3 layer has been shown to yield improved performance compared to single devices with a ZnO layer. This structure yielded an increased FF of 53% compared to 22% from the previous device, improving the J_{sc} from 43.66 A/m^2 to 76 A/m^2 while improving the V_{oc} from 0.349 V to 0.57 V. The power density of the device in the maximum power point (*MPP*) is 2.29 mW/cm^2.

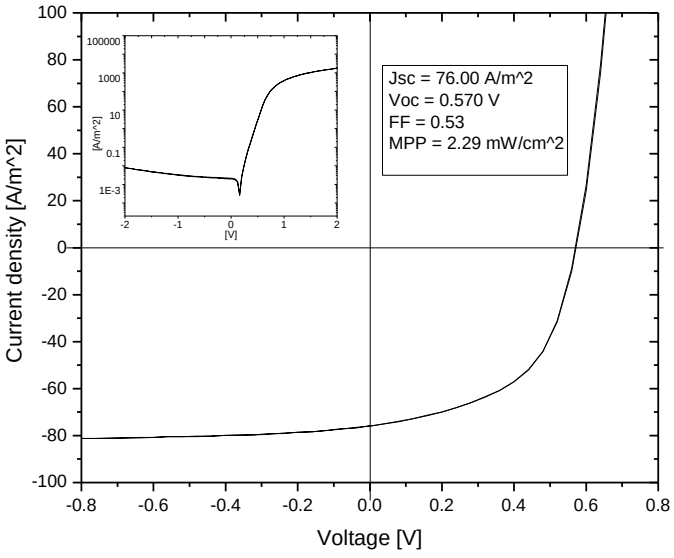

Figure 4.15. Current density – voltage characteristics of single cells with MoO3.

4.5 Organic tandem solar cells with MoO3/Ag/MoO3 as an intermediate layer

A polymer tandem solar cell containing two sub-cells in a parallel configuration was considered. This configuration generally is capable of producing higher currents and does not have the problem of optimization of the layer thickness of the sub-cells in a serial configuration. The device structure for the studied tandem solar cell with solution processed sub-cells is shown in Figure 4.16. The proposed geometry for this tandem cell is an inverted structure with P3HT:[60]PCBM as wide band gap front cell and a conventional structure with PCPDTBT:[60]PCBM as small band gap back cell. We propose a MoO_3/Ag/MoO_3 middle contact to separate and connect the two sub-cells.

The complementary absorption band of the donor materials used for each sub-cell (P3HT and PCPDTBT) leads to coverage of the whole visible range of the solar spectrum (up to 900 nm). A drawback of the conventional device structure is that the ITO/PEDOT:PSS interface is unstable and has an adverse affect on organic device performance over time. One way of overcoming this drawback is using inverted devices utilizing an evaporated metal oxide/ metal anode (e.g. MoO_3/Al) instead of PEDOT:PSS. An electrically conductive and transparent cathode should be placed on the ITO and a suitable anode should be placed on top of the active layer of the front cell. Thus, Zinc oxide (ZnO) as a low work function material was used as a transparent cathode. As an anode, a transparent layer of molybdenum trioxide (MoO_3) was used.

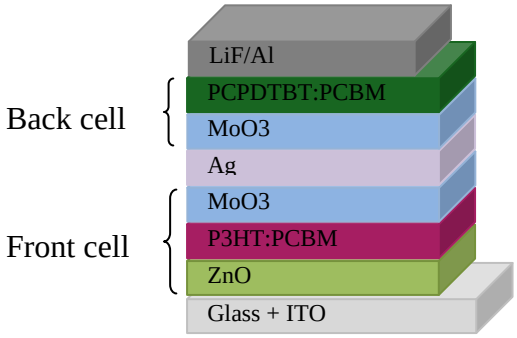

Figure 4.16. Device layout of the studied polymer tandem solar cell with solution processed sub-cells.

In order to determine the performance and electrical characteristics of the studied devices, current-voltage measurements were performed, both in dark and under illumination. The results of current density to voltage (*J–V*) characteristics measurements for the studied tandem solar cell are shown in Figure 4.17.

This studied polymer tandem solar cell reached fill factors of around 0.44, with open circuit voltages of 476 mV, short circuit currents of about 31.03 A/m^2 and the power density of the device in the maximum power point (*MPP*) is 0.65 mW/cm^2.

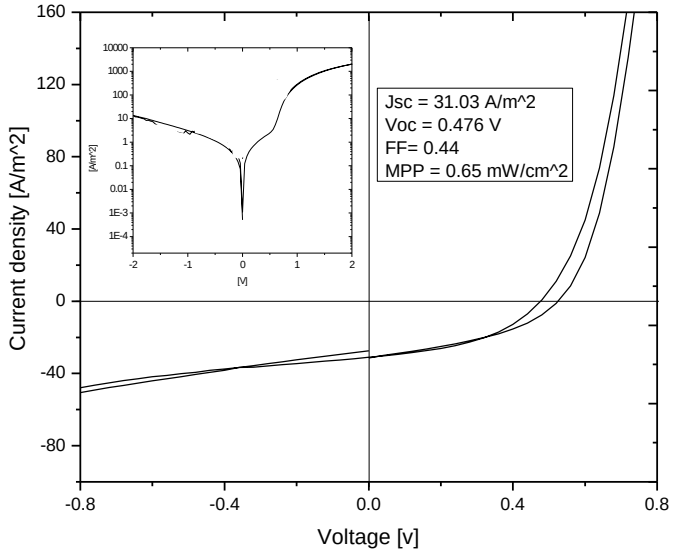

Figure 4.17. Current density to voltage characteristics of the tandem cell with MoO_3/Ag/MoO_3 middle contact

For more investigation, IPCE measurements of single (P3HT:PCBM blend and PCPDTBT:PCBM) and tandem (P3HT:PCBM / MoO_3/Ag/MoO_3 / PCPDTBT:PCBM) cells were performed. The IPCE is defined as the number of photogenerated charge carriers contributing to the photocurrent per incident photon. The incident-photon-to-current-efficiency (IPCE) measurement gives the spectral resolution of the photocurrent. Light coming through narrow band-pass filters is focused onto a solar cell and the current can be measured at a certain wavelength.

It can be observed that the curve of the tandem cell in the region between 600 and 800 nm has a peak with a maximum IPCE of ~23% at 680 nm. It shows that this curve just

contains the curve of the back cell and the IPCE of this device is consistent with the IPCE of the PCPDTBT:PCBM single cell. Possibly the bottom cell is short-circuited by the solution deposition of the top cell. It means that in this structure just the top cell works (Figure 4.18). Therefore, the need for a better control over the processing conditions of the tandem cell to have a closed interlayer after the first cell is obvious.

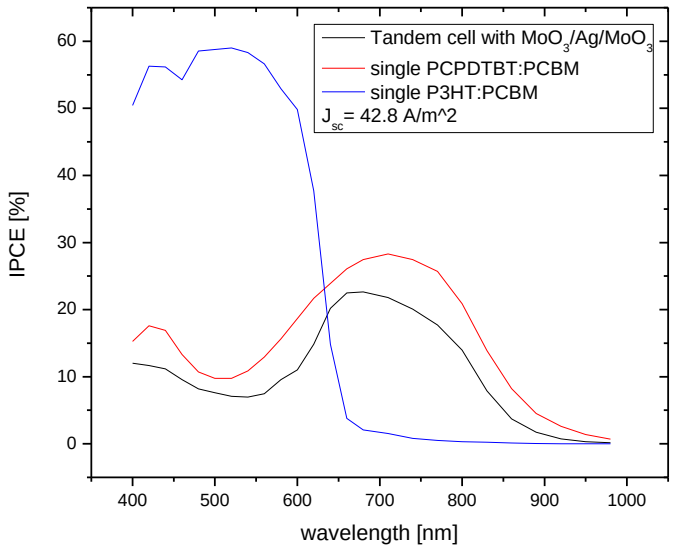

Figure 4.18. IPCE measurements of single and tandem cells with MoO_3/Ag/MoO_3 middle contact.

4.6 Optimizing organic tandem solar cells

4.6.1 The effect of increasing the thickness of molybdenum oxide layer on the performance of tandem solar cells

It is expected that better performance can be achieved with more tuning of the parameters of the intermediate layer. Therefore, a logical thing to do is to increase the thickness of the intermediate layer, because it may stop solvent from penetrating down through the structure. In order to achieve better performance, the thickness of the first and second MoO_3 layer was varied from 10 and 20 to 20 and 30 respectively. It can be observed from Figure 4.19 that the results show a similar tendency and they are not remarkably different from the previous results. It might be due to the fact that the MoO_3 layer is porous. Since

increasing the MoO_3 layer thickness does not result in increased performance, it was considered to replace this layer.

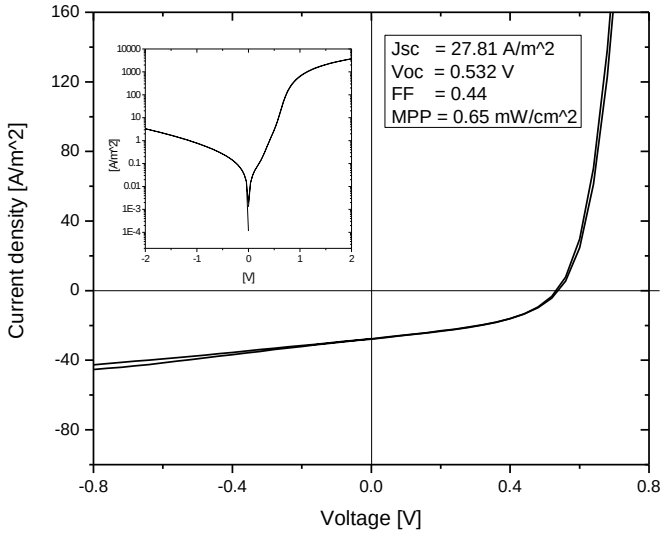

Figure 4.19. Current density to voltage characteristics of the tandem cell with MoO_3/Ag/MoO_3 middle contact.

4.6.2 The effect of using V_2O_5/Ag/ MoO_3 as the intermediate layer on the performance of tandem solar cells

In the next step, the first MoO_3 layer was replaced with V_2O_5. The cell was processed onto a glass/ITO substrate covered by a ZnO layer. For the front cell a layer of P3HT:PC_{60}BM was used. The V_2O_5 interlayer was spin coated. This was followed by the deposition of a Ag layer and a MoO_3 layer. On top of the interlayer a layer of PCPDTBT:PCBM as the back cell was spin coated. Finally the top electrode of LiF and Al is evaporated onto the device, resulting in a device structure of ITO/ZnO/P3HT:PCBM/V_2O_5/Ag/ MoO_3/PCPDTBT:PCBM/LiF/Al.

The performance of the above-mentioned tandem device in the dark and under illumination was measured and the results of the *J–V* measurements of the tandem cell are depicted in Figure 4.20. As can be seen, comparing the results with the previous tandem device it is obvious that this structure gives an unusual result. It can be observed

from Figure 4.21 that the IPCE has a maximum of ~45% at 500 nm which consistent with the IPCE of a P3HT:PCBM single cell. The IPCE spectra demonstrates that in this structure just the front cell works, possibly the surface roughness of this interlayer causes a short-circuit in the back cell.

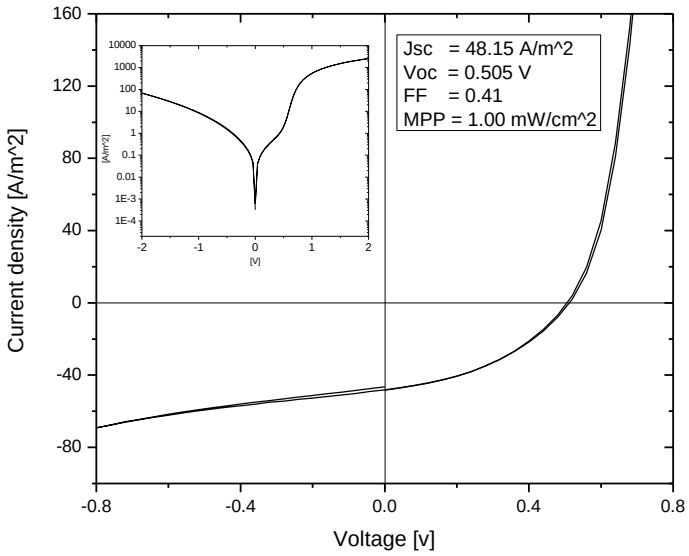

Figure 4.20. Current density to voltage characteristics of the tandem cell with V_2O_5/Ag/ MoO_3 middle contact.

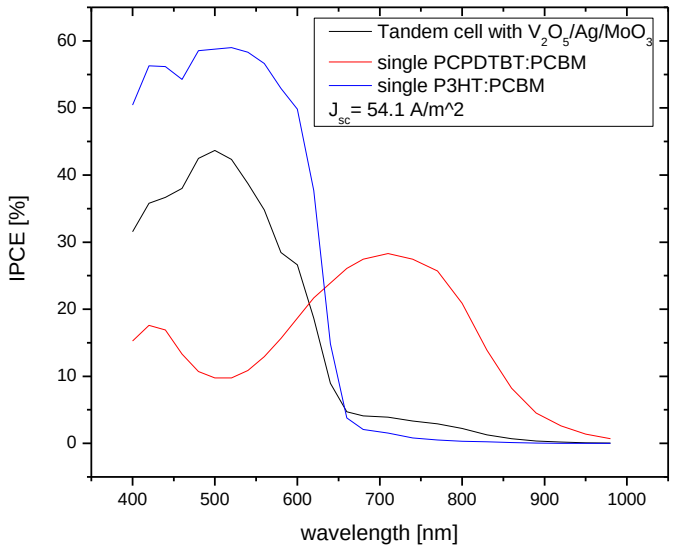

Figure 4.21. IPCE measurements of single and tandem cells with V_2O_5/Ag/ MoO_3 middle contact.

4.6.3 Investigating performance of sub-cells in studied organic tandem solar cells

To investigate further the performance of organic tandem cells with MoO_3/Ag/MoO_3 middle layer, a single configuration solar cell was fabricated and I-V characteristics were measured. The structure of the device is given in Figure 4.22. The performance of the above-mentioned single device in the dark and under illumination was measured and the results of the current density to voltage characteristics measurements of the device are depicted in Figure 4.23. Previously, the results for the current density to voltage (*J*–*V*) characteristics measurements of the device with the structure of ITO/ZnO/P3HT:PCBM/ MoO_3/Ag were shown in Figure 4.15.

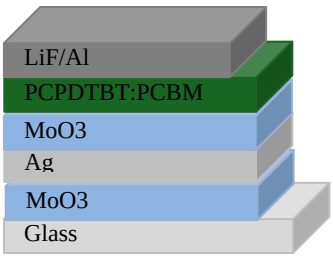

Figure 4.22. Device structure of studied single solar cells.

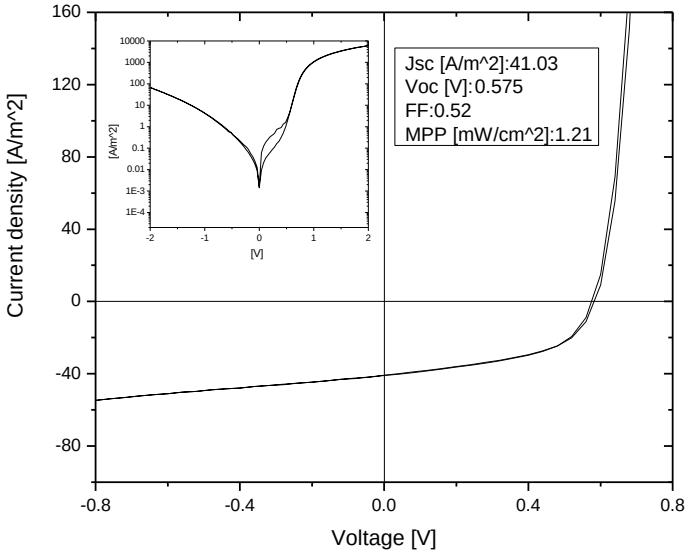

Figure 4.23. Current density to voltage characteristics of the single cell with PCPDTBT:PCBM.

As a consequence, it is found from the above results that both sub-cells work properly. This observation clearly demonstrates that in order to improve the performance of tandem solar cells with a $MoO_3/Ag/MoO_3$ middle layer, better control over the processing conditions is needed. Therefore, several experiments were carried out by changing the thickness of the silver layer in the $MoO_3/Ag/MoO_3$ interlayer. Another very interesting result of this structure is that the performance compares well to devices with an ITO anode (MPP = 1.6 mW/cm^2)

4.6.4 The effect of increasing the thickness of silver layer on the performance of tandem solar cells

A similar approach was taken here and tandem cell devices with a $MoO_3/Ag/MoO_3$ middle layer with a larger thickness of the silver layer were fabricated and the current - voltage curves of these devices were characterized. The results of the J-V characteristics measurements are shown in Figure 4.24. The results obtained from these devices yield better performance than those obtained in previous sections.

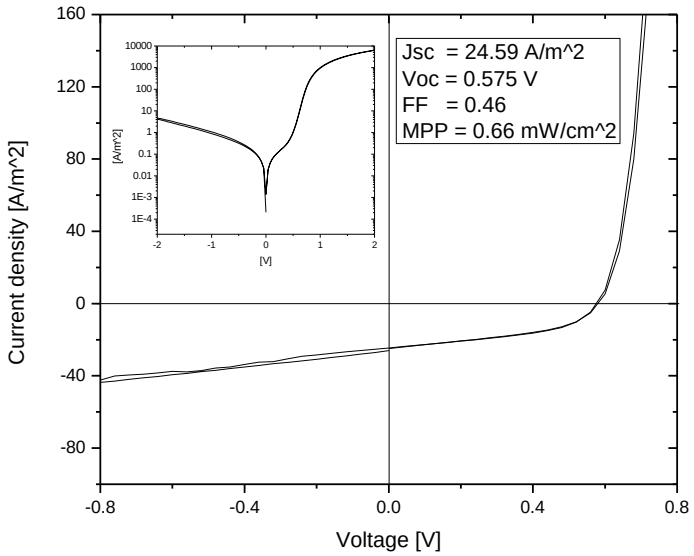

Figure 4.24. Current density to voltage characteristics of the tandem cell with $MoO_3/Ag/MoO_3$ middle contact with 10 nm silver layer thickness.

Figure 4.25 compares the incident photon-to-current collection efficiency (IPCE) spectrum of different tandem cell devices with different middle layers. Surprisingly, MoO_3/Ag(10nm)/ MoO_3 (green) yields a better results compared to the other two devices.

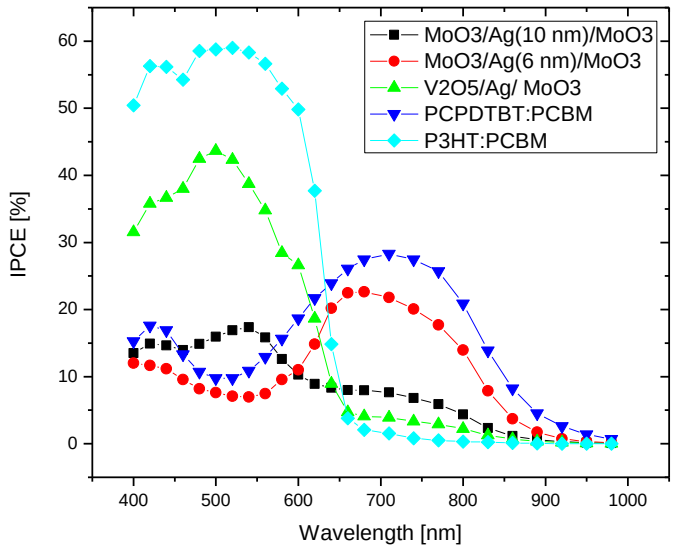

Figure 4.25. IPCE measurements of different tandem cell devices

It can be observed that, unlike the other two IPCE curves, the curve of the tandem cell with a MoO_3/Ag(10nm)/MoO_3 interlayer contains two maxima at 540 nm and 680 nm which is consistent with the IPCE of two individual single cells (P3HT:PCBM and PCPDTBT:PCBM). Additionally, it is found from the IPCE spectra that in this structure both cells produce photocurrent. It should be noted that this configuration shows the same V_{oc} as both bottom and top cells (0.57 V). An increased Ag film thickness seems to protect the bottom cell better, since both sub-cells contribute to the photocurrent. However because of the extra optical loss, the quantum efficiency is lower overall.

Improvements may be achieved through more investigation in these structures, in particular regarding the optimization of the middle layer of these devices.

5 Conclusions

During this work a parallel-connected organic tandem photovoltaic structure has been demonstrated and tested with various intermediate layers. Some experimental innovations have been established to overcome technological problems during processing of the multilayer structure. MoO_3/Ag/MoO_3 proves to be an outstanding multilayer as a transparent anode for fabricating organic tandem cells. Organic tandem solar cells based on MoO_3/Ag/MoO_3 as the intermediate layer are demonstrated to achieve good performance. Increased Ag film thickness seems to protect the bottom cell better, since both sub-cells contribute to the photocurrent. The open-circuit voltage V_{oc} for the tandem cell device is the same as the V_{oc}'s of the individual cells. Therefore, the MoO_3/Ag/ MoO_3 middle contact serves as a stable foundation that enables the fabrication of the second cell to complete the tandem cell architecture without destroying or dissolving the underlying layers. The loss of overall quantum efficiency might be explained by the extra optical loss. We expect that the performance of organic tandem photovoltaic devices can be improved by optimizing the optical properties of the MoO_3/Ag/MoO_3 multilayer to achieve high conductivity and transparency.

A ZnO/Ag/ZnO layer as a high quality transparent cathode is demonstrated to achieve excellent peak optical transmittance of 80% and could be reproduced through a simple manufacturing process and convenient procedure. We have shown that the electrical operation of single solar cells with a thin MoO_3/Ag/MoO_3 multilayer anode and without ITO perform well (MPP = 1.21 mW/cm^2) compared to devices with an ITO anode (MPP = 1.6 mW/cm^2). Furthermore, higher performance can be achieved by optimizing the optical properties of the MoO_3/Ag/MoO_3 multilayer.

6 Acknowledgement

First of all, I would like to thank Prof. Paul Blom for giving me the opportunity to do my master research project in his group, as well as giving me guidance, advice, and useful directions during this time. I had an opportunity for doing my research in a friendly environment and a nice group at this university.

Special thank to my daily supervisor Paul de Bruyn for all his ideas, help, and encouragement, and for making my research an enjoyable experience! I would also like to thank Jan Harkema for his invaluable technical help and his effort for making very nice environment in clean room for students. Furthermore I would like to express my appreciation to the entire group member for the good time and friendly atmosphere.

References

[1] D. Wfhrle, D. Meissner, Adv. Mater. **3** (1991) 129.

[2] C.W. Tang, Appl. Phys. Lett. **48** (1986) 183.

[3] P. Peumans, A. Yakimov, S.R. Forrest, J. Appl. Phys. **93** (2003) 3693.

[4] S.E. Shaheen, C.J. Brabec, N.S. Sariciftci, F. Padinger, T. Fromerz,, J.C. Hummelen, Appl. Phys. Lett. **78** (2001) 841.

[5] G. Yu, J. Gao, J.C. Hummelen, F. Wudl, A.J. Heeger, Science **270** (1995) 1789.

[6] C.J. Brabec, F. Padinger, N.S. Sariciftci, J.C. Hummelen, J. Appl. Phys. **85** (1999) 6866.

[7] J. Gilot, M. M. Wienk, and R. A. J. Janssen, Appl. Phys. Lett. **90** (2007), 143512.

[8] C. K. Chiang, C. R. Fincher, Y. W. Park, A. J. Heeger, H. Shirakawa, E. J. Louis, S. C. Gau, and A. G. MacDiarmid: Electrical conductivity in doped polyacetylene. *Phys. Rev. Lett.*, Vol. 39, 1098, 1977.

[9] Shirakawa H., Louis E.J., Macdiarmid A.G., et al. *J.C.S. Chem. Comm*. **16** 578-580 (1977).

[10] Blom P.W.M., Valentin D. M., L. Jan Anton Koster, and Denis E. Markov, *Adv. Mater.* ....(2007).

[11] Hans-Jürgen Prall, TANDEM SOLAR CELLS, PhD thesis, Johannes Kepler Universität Linz (2005).

[12] Jin Young Kim, et al., Science **317** (2007), 222.

[13] Hadipour A., de Boer B., Wildeman J., Kooistra F.B., Hummelen J.C., Turbiez M.G.R., Wienk M.M., Janssen R.A.J. and Blom P.W.M. *Adv. Funct. Mater. **16 (*** 2006), 1897.

[14]Gilot J., Wienk M.M., Janssen R.A.J., *Appl. Phys. Lett.*, **90**, 143512 (2007)

[15] K. Sugiyama, H. Ishii, Y. Ouchi, and K. Seki, ‘‘Dependence of Indium-Tin-Oxide Work Function on Surface Cleaning Method as Studied by Ultraviolet and X-ray Photoemission Spectroscopies,’’ J. Appl. Phys., vol. 87, no. 1, pp. 295_298, 2008.

[16] J. Tang, X. Wang, L. Brzozowski, D. A. R. Barkhouse, R. Debnath, L. Levina, and E. H. Sargent, ‘‘Schottky Quantum Dot Solar Cell Stable in Air Under Solar Illumination,’’ Adv. Mater, vol. 22, no. 12, pp. 1398_1402, 2010.

[17] Y. Kim, S. A. Choulis, J. Nelson, D. D. C. Bradleyl, S. Cook, and J. R. Durrant, ‘‘Device Annealing E_ect in Organic Solar Cells with Blends of Regioregular Poly(3- Hexylthiophene) and Soluble Fullerene,’’ Adv. Mater, vol. 86, no. 6, pp. 063502 _063502_3, 2009.

[18] S.K. Hau, H.L. Yip, H. Ma, A.K.Y. Jen, Appl. Phys. Lett. 93 (2008) 233304.

[19] F.C. Krebs, Sol. Energy Mater. Sol. Cells 92 (2008) 715.

[20] A.K.K. Kyaw, X.W. Sun, C.Y. Jiang, G.Q. Lo, D.W. Zhao, D.L. Kwong, Appl. Phys. Lett. 93 (2008) 221107.

[21] P. de Bruyn, D.J.D. Moet, P.W.M. Blom. Org. Electronics. **11** (2010) 1419-1422.

[22] D.J.D. Moet, Enhanced performance of single and double junction plastic solar cells, PhD thesis, University of Groningen (2011)